Journal of Solid State Chemistry

Volume 199, Pages 1-344 (March 2013)

symmetry increase on cooling. ► Damping effect present larger contribution of orientational mechanism in CW than in the RW system.

Synthesis of hollow spherical tantalum oxide nanoparticles and their photocatalytic activity for hydrogen production

Original Research Article
Pages 15-20
Sen Lin, Lei Shi, Hisao Yoshida, Mingrun Li, Xiaodong Zou

Highlights

► Hollow spherical tantalum oxide (HSTaO) nanoparticles were synthesized using the nonionic triblock copolymer F127 as template in an ethanol aqueous medium. ► Morphology, structure and porosity of HSTaO nanoparticles were characterized. ► HSTaO showed high photocatalytic activity similar to that of bulk Ta_2O_5, but higher stability than bulk Ta_2O_5.

Crystal structure modeling, electrical and thermal characterization of triple molybdates $RbCrTi_{0.5}(MoO_4)_3$ (*R*=Fe, Cr)

Original Research Article
Pages 21-26
Sesegma G. Dorzhieva, Bair G. Bazarov, Alexey K. Subanakov, Jibzema G. Bazarova

Highlights

► The new triple molybdates of $RbRTi_{0.5}(MoO_4)_3$ (*R*=Fe, Cr) were synthesized. ► Their crystal structures have been refined by Rietveld analysis. ► This compounds have a superionic phase transition at temperature above ~450 °C. ► $RbCrTi_{0.5}(MoO_4)_3$ has rather high conductivity, approaching 0.57×10^{-2} S cm^{-1}.

Theoretical study of phase stability, magnetization and lattice vibrations of $Fe_{23}CB_6$ structure with $Cr_{23}C_6$ prototype

Original Research Article
Pages 27-33
Zhen-Feng Zhang, Ping Qian, Ya-Ping Li, Jin-Chun Li, Jiang Shen, Nan-Xian Chen

Highlights

► New crystal structure $Fe_{23}CB_6$ predicted via pair potentials based on lattice-inversion method. ► Phase stability and site preference substitution of Fe23−*x*T*x*B6 are analysed. ► The magnetic

moments of $Fe_{22}NiB_6$, $Fe_{23}C_6$, $Fe_{23}B_6$ and $Fe_{23}CB_6$ are calculated. ► The phonon densities of states of Fe22TB6, Fe23C6, Fe23B6 and Fe23CB6 are first evaluated.

Influence of the network modifier on the characteristics of $MSnO_3$ (M=Sr and Ca) thin films synthesized by chemical solution deposition

Original Research Article
Pages 34-41
M.C.F. Alves, R.M.M. Marinho, G.P. Casali, M. Siu-Li, S. Députier, M. Guilloux-Viry, A.G. Souza, E. Longo, I.T. Weber, I.M.G. Santos, V. Bouquet

Highlights

► $MSnO_3$ (M=Ca, Sr) thin films were synthesized by CSD on single crystal. ► The influence of Ca/Sr on structural and microstructural properties was studied. ► Epitaxial films were obtained on STO and polycrystalline films on sapphire. ► The network modifier influenced the crystallization process of the films. ► The short-range order was modified by the epitaxial growth.

Tuning structural topologies of five photoluminescent Cd(II) coordination polymers through modifying the substitute group of organic ligand

Original Research Article
Pages 42-48
Feng Guo, Baoyong Zhu, Guilan Xu, Miaomiao Zhang, Xiuling Zhang, Jian Zhang

Highlights

► Five new Cd(II) complexes have been synthesized and characterized. ► The structural diversities is due to the adjustment of substituted groups of ligands and pH values. ► These complexes show good luminescent properties.

Influence of post-treatment temperature of TNTa photoelectrodes on photoelectrochemical properties and photocatalytic degradation of 4-nonylphenol

Original Research Article
Pages 49-55
Yanjun Xin, Huiling Liu, Junjing Li, Qinghua Chen, Dong Ma

Highlights

► Effect of annealed temperature on Morphology of TNTa photoelectrodes. ► Effect of annealed temperature on crystal structure of TNTa photoelectrodes. ► Effect of annealed temperature on Optical and PECH properties. ► PC and PEC degradation activity of 4-NP by TNTa photoelectrodes. ► Analysis of degradation mechanism of 4-NP on TNTa photoelectrodes.

Novel bismuth oxophosphate halides $[Bi_8O_8][BiO_2](PO_4)_2X$ (*X*=Cl, Br) based on oxocentered 2D blocks and their relationships to the Aurivillius phases

Original Research Article
Pages 56-61
Michael S. Kozin, Almaz Aliev, Marie Colmont, Olivier Mentré, Oleg I. Siidra, Sergey V. Krivovichev

Highlights

► Two novel Bi oxohalides have been obtained by the solid-state reaction method. ► The substructure consists of OBi_4 tetrahedra and OBi_3 triangles. ► The topology of this oxocentered O–Bi structural unit is two-dimensional. ► Units are related to the $[O_2Bi_2]^{2+}$ layers typical for the Aurivillius type compounds.

Crystal structure of Li_4ZnTeO_6 and revision of $Li_3Cu_2SbO_6$

Original Research Article
Pages 62-65
V.B. Nalbandyan, M. Avdeev, M.A. Evstigneeva

Highlights

► Li_4ZnTeO_6 has been prepared and refined by powder neutron diffraction. ► It is monoclinic C2/m isostructural with $Li_3M_2SbO_6$ (M□Zn, Cu, Ni and Co). ► $Li_3Cu_2SbO_6$ reported originally as C2/c is reindexed with halved unit cell volume.

β-HfCuGe—A new polymorph of HfCuGe with a novel structure type

Original Research Article
Pages 66-70
Leslie M. Schoop, Jared M. Allred, Ni Ni, D. Hirai, Julia Krez, Michael Schwall, Huiwen Ji, Mazhar N. Ali, R.J. Cav

Highlights

► Layered intermetallic compound. ► BCC Hf layers and square planar CuGe network. ► Metallic conductor and paramagnetic.

Solid solutions of platinum(II) and palladium(II) oxalato-complex salt as precursors of nanoalloys

Original Research Article
Pages 71-77
A.V. Zadesenets, T.I. Asanova, E.S. Vikulova, E.Yu. Filatov, P.E. Plyusnin, I.A. Baidina, I.P. Asanov, S.V. Korenev

Highlights

► Solid solution of isomorphous complexes as single-source precursors for Pd–Pt nanoalloys.► Simultaneous reduction of metals leading to single phase nanoalloy. ► Dependence of particle size on heating rate and atmosphere. ► Uniform distribution of components in the particles.

Evolutionary search for $BiInS_3$ crystal structure and predicting its second-order nonlinear optical property

Original Research Article
Pages 78-83
Chen-sheng Lin, Wen-dan Cheng, Zhong-zhen Luo, Guo-liang Chai

Highlights

► $BiInS_3$ crystal structure was predicted by evolutionary algorithm. ► Electronic structure of $BiInS_3$ was studied by density functional theory. ► Nonlinear optical property was calculated for $BiInS_3$. ► $BiInS_3$ has large second-harmonic generation coefficient in mid-infrared region.

The composite structure of mixed τ-$(Ag, Cu)_xV_2O_5$ bronzes—Evidence for *T* dependant guest-species ordering and mobility

Original Research Article
Pages 84-89
Wilfred Hermes, Mickaël Dollé, Patrick Rozier, Sven Lidin

Highlights

► Insertion/removal of Ag/Cu understood from a composite perspective. ► Ordering of Cu/Ag in an incommensurate composite. ► Complex thermal behaviour. ► Extreme compositional dependence of order.

Investigation on the thermoelectric properties of nanostructured $Cr_{1-x}Ti_xSi_2$

Original Research Article
Pages 90-95
S. Karuppaiah, M. Beaudhuin, R. Viennois

Highlights

► Nano-$CrSi_2$ Ti-doped pellets have been obtained without any residual phases. ► Thermal conductivity is decreased by a factor 10 when the grain size is about 50 nm. ► Experimental results and simulation of the structure stability are in good agreement. ► The electrical resistivity is strongly reduced by a factor 3 at 600 K by Ti-doping. ► We report an enhancement of the power factor by a factor 2 for 10% Ti-doping.

Characteristic features of the structural properties, phase transitions, and ferroelastic properties in $LiK_{1-x}Rb_xSO_4$ (x=0, 0.2, and 1) crystals

Original Research Article
Pages 96-101
Ae Ran Lim, Ho Hyoun Kim, Moohee Lee

Highlights

► The effects of the random distribution of the Rb substitutional. ► the transition temperatures by presence of rubidium ions in the potassium sites. ► the ferroelastic properties.

Structural and magnetic investigation of Fe^{3+} and Mg^{2+} substitution into the trigonal bipyramidal site of $InGaCuO_4$

Original Research Article
Pages 102-108
Rosa Grajczyk, Romain Berthelot, Sean Muir, A.W. Sleight, M.A. Subramanian

Highlights

► Solid solutions of $InM^{3+}M^{2+}O_4$ (M^{3+}=Ga, Fe; M^{2+}=Cu, Mg) have been synthesized. ► A complete solid solution was achieved for the hexagonal $InGa_{1-x}Fe_xCuO_4$. ► Samples with high Fe/Mg content contained both the hexagonal and spinel phases. ► Spin glass magnetic interactions were observed in the hexagonal samples.

The preferential growth of ZnS on ZnOnanorods

Original Research Article
Pages 109-115
Haridas Kumarakuru, David Cherns

Graphical abstract

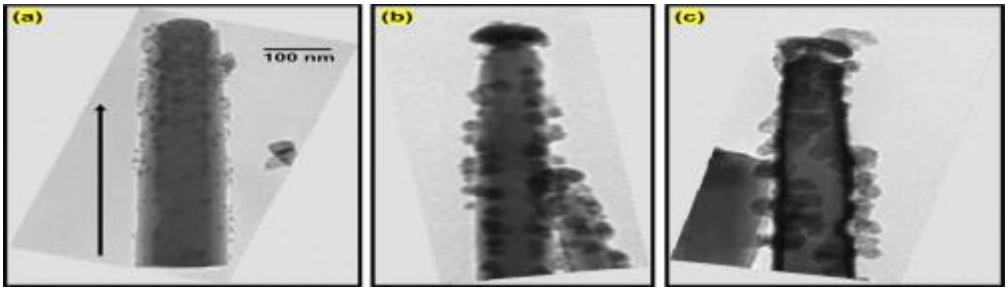

Highlights

► The mechanism of sulphide growth on (0001) ZnO nanorods is examined by TEM and SEM. ► The reaction occurs on (0001) and on the lines of intersection of the $\{10\bar{1}0\}$. ► The reaction involves Zn migration to reaction sites via surface diffusion. ► A voided interlayer between ZnS and ZnO may be explained by the Kirkendall effect.

Novel light-conversion hybrids of SBA-16 functionalized with rare earth (Eu^{3+}, Nd^{3+}, Yb^{3+}) complexes of modified 2-methyl-9-hydroxyphenalenone and 1,10-phenanthroline

Original Research Article
Pages 116-122
Yan-Jing Gu, Bing Yan, Xiao-Fei Qiao

Highlights

► Novel functionalized derivative is used for chemical linkages. ► New mesoporous lanthanide hybrids of SBA-16 are assembled. ► Luminescence and light conversion in the visible and NIR regions are achieved.

Phase homology in new layered mixed Li, *M* (*M*=Mg, Cu, Cd, Pb, Bi) bismuth oxophosphates and oxoarsenates

Original Research Article
Pages 123-128

M.S. Kozin, M. Colmont, D. Endara, A. Aliev, M. Huvé, O.I. Siidra, S.V. Krivovichev, O. Mentré

Graphical abstract

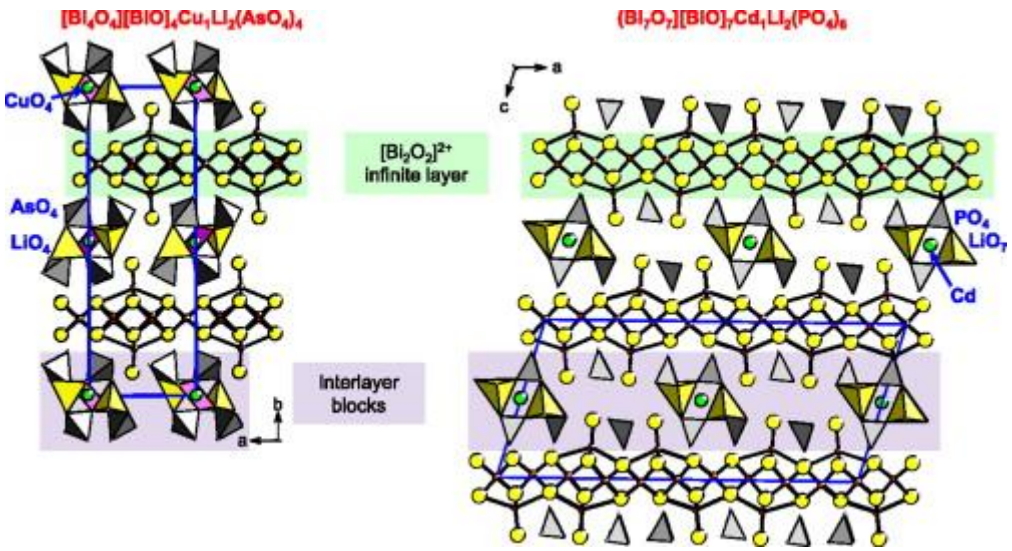

Highlights

► Two new bismuth oxophosphate were synthesized. ► Crystal structure were solved thanks to single crystal X-Ray diffraction. ► They show infinite $[Bi_2O_2]^{2+}$ layers surrounded by XO_4 (*X*=*P*, As), LiO_x and MO_y connected entities. ► The insertion of lithium drastically changed the classical topology observed in related Aurivillius compounds.

A series of inorganic aggregates composed of $[MnV_{13}O_{38}]^{7-}$ polyoxoanions and transition metal cations

Original Research Article
Pages 129-133
Qing Lan, Huaqiao Tan, Ding Liu, Enbo Wang

Highlights

► The polyoxoanions $[MnV_{13}O_{38}]^{7-}$ has been investigated scarcely. ► A series of $[MnV_{13}O_{38}]^{7-}$-based extended frameworks have been reported. ► The compounds are the first TM supported $[MnV_{13}O_{38}]^{7-}$-based materials.

Formation processes of high-dimensional Mo□O frameworks in tetrakis(2-hydroxypropane-1,3-diaminium) hexatriacontamolybdate hydrate $(C_3H_{12}N_2O)_4[Mo_{36}O_{112}(H_2O)_{16-m}]\cdot nH_2O$ crystals: Solid-phase structural conversions under restricted dehydration conditions

Original Research Article
Pages 134-140
Kazuo Eda, Tatsuya Koduka, Yuichi Iriki, M. Stanley Whittingham

Highlights

► Structural diversity of the compound $(C_3H_{12}N_2O)_4[Mo_{36}O_{112}(H_2O)_{16-m}]\cdot nH_2O$ was revealed. ► Seven structural phases with Mo□O framework structures of various dimensionalities were found. ► Seven phases showed snapshots concerning formation processes of high-dimensional frameworks. ► Initially formed hydrogen bonds guided us to obtain the compounds with high-dimensional frameworks. ► Restricted dehydration enabled us to obtain the compounds with high-dimensional frameworks.

Tetragonal-antiprismatic coordination of transition metals in intermetallic compounds: ω_1-Mn_6Ga_{29} and its structuralrelationships

Original Research Article
Pages 141-148
Iryna Antonyshyn, Yurii Prots, Irene Margiolaki, Marcus Peter Schmidt, Olga Zhak, Stepan Oryshchyn, Yuri Grin

Highlights

► The crystals of new phase ω_1-Mn_6Ga_{29} are grown from Ga flux. ► Single-crystal diffraction data is obtained from the twinned specimen. ► The ω_1-Mn_6Ga_{29} structure represents a new prototype. ► Main building unit is distorted monocapped tetragonal antiprism $[MnGa_{8+1}]$. ► The structural peculiarities of ω_1-Mn_6Ga_{29} and related structures are discussed.

A first-principles study on chromium sesquioxide, Cr_2O_3

Original Research Article
Pages 149-153

C. Wessel, R. Dronskowsk

Highlights

► Ab initio calculations predict the [Rh_2O_3(II)] type as a possible Cr_2O_3 high-pressure polymorph. ► Phonon calculations indicate that Cr_2O_3 adopting the [Rh_2O_3(II)] type is dynamically stable. ► The calculation of the effective coordination number according to Brunner and Schwarzenbach yields a preferred coordination number larger than 5.5 for high-pressure Cr_2O_3. ► The bixbyite type is identified as an energetically promising candidate for a new Cr_2O_3 polymorph at ambient pressure.

Crystal structure and oxygen content of the double perovskites $GdBaCo_{2-x}Fe_xO_{6-\delta}$

Original Research Article
Pages 154-159
D.S. Tsvetkov, I.L. Ivanov, A.Yu. Zuev

Highlights

► Origin of the *Pmmm-P4/mmm* transition in $GdBaCo_{2-x}Fe_xO_{6-\delta}$ depends significantly on iron content. ► The iron solubility limit in $GdBaCo_{2-x}Fe_xO_{6-\delta}$ is equal to 0.65. ► Oxygen content in $GdBaCo_{2-x}Fe_xO_{6-\delta}$ at given temperature increases with Fe content.

Nickel segment-length dependent magnetic properties of Au–Ni–Au nanowires at low temperature fabricated by electrochemical deposition

Original Research Article
Pages 160-163
S. Ishrat, K. Maaz, Kyu Joon Lee, Myung-Hwa Jung, Gil-Ho Kim

Highlights

► Au–Ni–Au nanowires with various Ni segments were synthesized in AAO templates. ► Structural analysis confirmed the formation of pure-phase, purely crystalline wires. ► Enhanced

magnetic anisotropy of the nanowires was obtained at low temperatures. ► While H_c and M_s as a function of l followed decreasing trends at 300 K and 2 K.

Glucose-assisted hydrothermal preparation and catalytic performance of porous $LaFeO_3$ for toluene combustion

Original Research Article
Pages 164-170
Kemeng Ji, Hongxing Dai, Jiguang Deng, Liyun Song, Shaohua Xie, Wen Han

Highlights

► 3D porous $LaFeO_3$ is prepared by the glucose-assisted hydrothermal method. ► A suitable hydrothermal temperature is needed for 3D porous $LaFeO_3$ formation. ► 3D porous $LaFeO_3$ is high in surface area and O_{ads} content and good in reducibility. ► 3D porous $LaFeO_3$ performs well in the combustion of toluene. ► Catalytic activity is governed by surface area, O_{ads} concentration, and reducibility.

The system Ta–V–Si: Thermodynamic modeling

Original Research Article
Pages 171-180
P. Broz, A.U. Khan, H. Niu, X.-Q. Chen, D. Li, J. Vrestal, J. Bursik, P. Rogl

Graphical abstract

Highlights

► Thermodynamic modeling of the Ta–V–Si system has been performed. ► Ground state phase stabilities of compounds using an *ab initio* approach are reported. ► The calculated energies of formation were included in the thermodynamic modeling. ► Thermodynamic optimization required thermodynamic remodeling of Ta–V and V–Si system. ► Good agreement of experimental results with thermodynamic calculations was received.

New cubic superstructure of titanium monoxide with double structure

imperfection

Original Research Article
Pages 181-188
A.I. Gusev

Highlights

► Cubic model of Ti_5O_5 ($Ti_5{\blacksquare}O_5{\square}=Ti_{90}{\blacksquare}_{18}O_{90}{\square}_{18}$) superstructure. ► The disorder–order Ti_xO_z (space group $Fm\bar{3}m$)—Ti_5O_5 (space group $Pm\bar{3}m$) phase transition channel. ► Distribution of Ti and O atoms and vacancies ■ and □ in the unit cell of cubic Ti_5O_5 ordered phase. ► Admissible sequences of transformaions connected with the formation of cubic and monoclinic Ti_5O_5 ordered phases.

Ternary rare-earth zinc arsenides *RE*Zn_2As_3 (*RE*=La–Pr) containing defect fluorite-type slabs

Original Research Article
Pages 189-195
Xinsong Lin, Stanislav S. Stoyko, Arthur Mar

Highlights

► *RE*Zn_2As_3 (*RE*=La–Pr) adopt new structure types. ► Fluorite-type slabs built of $ZnAs_4$ tetrahedra are deficient in Zn. ► Stacking of these slabs differs in the La vs. Ce or Pr members.

Simulation of the growth kinetics of boride layers formed on Fe during gas boriding in H_2-BCl_3 atmosphere

Original Research Article
Pages 196-203
M. Kulka, N. Makuch, A. Pertek, L. Małdziński

Highlights

► The model of growth kinetics of two-phase boride layer on pure Fe was proposed for gas boriding. ► The mass balance equations were formulated. ► The parabolic growth constants and the activation energies were determined. ► The diffusion annealing, carried out in order to obtain a single-phase boride layer, was analyzed. ► The time for the total elimination of FeB phase was calculated and compared to the experimental data.

Solvothermal synthesis, characterization and magnetic properties of α-Fe_2O_3 and Fe_3O_4 flower-like hollow microspheres

Original Research Article
Pages 204-211
Jing-San Xu, Ying-Jie Zhu, Feng Che

Graphical abstract

Flower-like hollow microspheres of α-Fe_2O_3 and Fe_3O_4 have been prepared by a solvothermal combined with precursor heat treatment method. α-Fe_2O_3 hollow microspheres exhibit a high coercivity value of 2738 Oe, and Fe_3O_4 hollow microspheres have a saturation magnetization of 58.3 emu g^{-1}.

Highlights

► Flower-like hollow microspheres of α-Fe_2O_3 and Fe_3O_4 are prepared. ► A solvothermal combined with heat treatment method has been demonstrated. ► The growth mechanism of the product is investigated. ► α-Fe_2O_3 hollow microspheres exhibit a high coercivity value.

Characterisation, phase stability and surface chemical properties of photocatalytic active Zr and Y co-doped anatase TiO_2 nanoparticles

Original Research Article
Pages 212-223
Andreas Mattsson, Christian Lejon, Snejana Bakardjieva, Vaclav Štengl, Lars Österlund

Graphical abstract

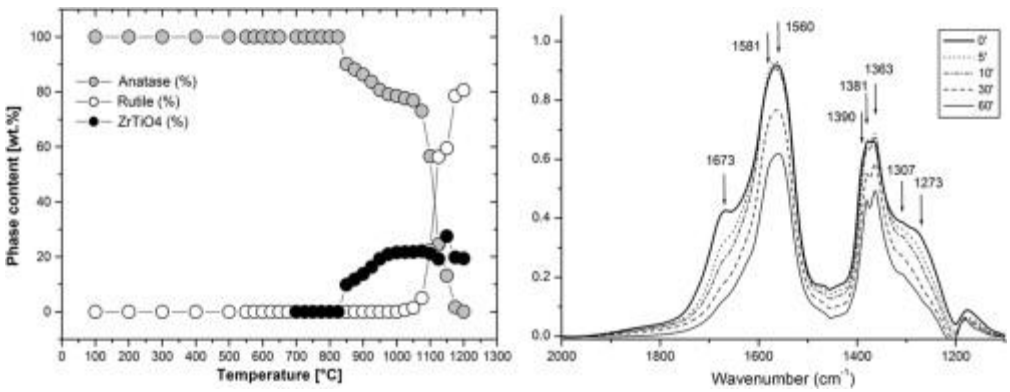

Highlights

► Precipitation of cations occurs upon anatase to rutile phase transformation. ► Doping increase surface acidity and affect the structure of the adsorbed formic acid. ► Photocatalytic degradation rates correlates with increased surface acidity.

Synthesis, characterization, and photocatalytic properties of BiOBr catalyst

Original Research Article
Pages 224-229
Yan Wang, Zhuqing Shi, Caimei Fan, Xiaowen Wang, Xiaogang Hao, Yongqing Chi

Graphical abstract

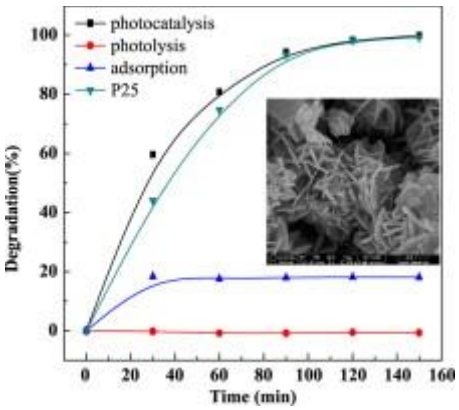

Highlights

► The BiOBr potocatalyst was synthesized by a simple hydrolysis method. ► This method is an environmental friendly preparation method. ► This method does not need high temperature calcinations. ► The photocatalytic activity of as-prepared BiOBr is as good as P_{25}-TiO_2. ► Photogenerated h^+ and ·OH play key roles in the photocatalytic degradation process.

Assembly of Cu/Ag-quinoxaline-polyoxotungstate hybrids: Influence of Keggin and Wells–Dawson polyanions on the structure

Original Research Article
Pages 230-239
Ying-Nan Chi, Feng-Yun Cui, Zheng-Guo Lin, Yan Xu, Xiao-Yu Ma, Pan-Pan Shen, Kun-Lin Huang, Chang-Wen Hu

Highlights

► The POM-based compounds **1**–**4** have been synthesized and characterized. ► Their electrochemistry properties have been studied. ► The volume and coordination ability of POMs play an important role in the assembly.

Re-examination of "Pb_3TeO_6": Determination of its correct composition as Pb_5TeO_8

Original Research Article
Pages 240-247
Christine Artner, Matthias Weil

Highlights

► Revision of the composition of previously reported "Pb_3TeO_6" as Pb_5TeO_8. ► Crystal structure determination of Pb_2TeO_5, Pb_5TeO_8, and Pb_6CdTeO_{10}. ► Correct relation between composition, crystal structure and physical properties of the compounds is reported. ► Revision of the space group of synthetic Pb_2TeO_5.

Color Point Tuning by Partial Ba^{2+} Substitution of Ca^{2+} in $(Ca_{1-x}Ba_x)_3(PO_4)_2$ Phosphor for White Light Emitting Diodes

Original Research Article
Pages 248-252
Yinqun Li, Hua Yu, Degang Deng, Youjie Hua, Shilong Zhao, Guohua Jia, Huanping Wang, Lihui Huang, Yinyan Li, Chenxia Li, Shiqing Xu

Highlights

► $(Ca_{1-x}Ba_x)_3(PO_4)_2$:Eu^{2+} phosphor could be effectively excited by UV chips (360–430 nm). ► the emission wavelength can be tuned in the range of 447–550 nm with different Ba^{2+}content. ► With the Ba^{2+} content increasing, the bandgap of $(Ca_{1-x}Ba_x)_3(PO_4)_2$ broadens from 5.5 to 5.9 eV.

Syntheses and crystal structures of three barium uranium sulfides

Original Research Article
Pages 253-257
Adel Mesbah, James A. Ibers

Graphical abstract

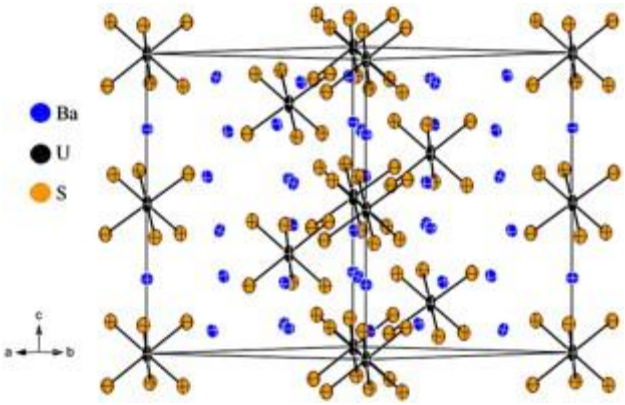

Highlights

► The barium uranium sulfides $Ba_{3.69}US_6$,$BaUS_3$, and BaU_2S_5 have been synthesized and characterized. ► $Ba_{3.69}US_6$ is a new mixed valent U^{4+}/U^{5+} compound. ► Dimensionality of these compounds decreases with increasing Ba–to–U content.

Influence of KOH-activated graphite nanofibers on the electrochemical behavior of Pt–Ru nanoparticle catalysts for fuel cells

Original Research Article
Pages 258-263
Seul-Yi Lee, Byung-Ju Kim, Soo-Jin Park

Highlights

► GNFs were activated chemically by KOH with a heat treatment. ► Chemical activation increased the available active surface of GNFs. ► It is due to the lower Pt–Ru particle size, higher SSA and oxygen functional groups. ► Thus, the Pt–Ru/K900-GNFs catalyst showed the highest electrochemical activity.

Study of the pseudo-ternary Ag_2S–As_2S_3–HgI_2 vitreous system

Original Research Article
Pages 264-270
R. Boidin, D. Le Coq, A. Cuisset, F. Hindle, J.-B. Brubach, K. Michel, E. Bychkov

Graphical abstract

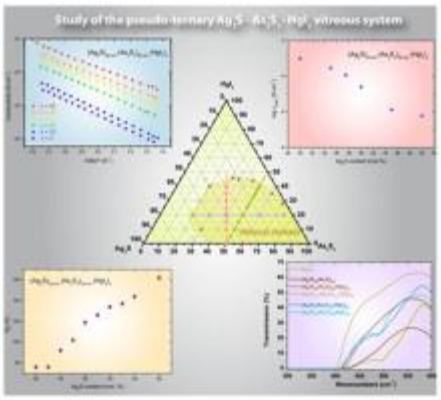

Highlights

► Studies of three glass series in the pseudo-ternary Ag_2S□As_2S_3□HgI_2 system. ► Investigation of some macroscopic properties of the Ag_2S□As_2S_3□HgI_2 glasses. ► HgI_2 contribution in the far-infrared transmission of the pseudo-ternary Ag_2S□As_2S_3□HgI_2 glasses. ► Characterization of the total conductivity of Ag_2S□As_2S_3□HgI_2 glasses.

Controlled synthesis of nitrogen-doped binary and ternary TiO_2 nanostructures with enhanced visible-light catalytic activity

Original Research Article
Pages 271-279
Ligang Gai, Qinghu Mei, Xiuquan Duan, Haihui Jiang, Guowei Zhou, Yan Tian, Xifeng Lu

Highlights

► Nitrogen-doped binary and ternary TiO_2 photocatalysts are controllably synthesized. ► The catalysts are prepared through a hydrazine-mediated solvothermal approach. ► The properties of the catalysts can be tuned by simply changing the reaction time. ► The catalysts exhibit enhanced visible-light photocatalytic activity compared to P25. ► The selected catalyst shows high photostability after reuse four times.

Facile fabrication of N-doped TiO_2 nanocatalyst with superior performance under visible light irradiation

Original Research Article
Pages 280-286
Jie Fu, Yanlong Tian, Binbin Chang, Fengna Xi, Xiaoping Dong

Graphical abstract

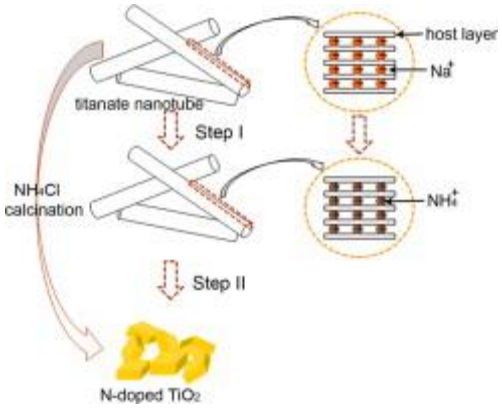

Highlights

► N-doped TiO_2 catalyst is synthesized by a facile and environment-conscious method. ► An inorganic ammonium salt and titanate nanotubes were used as Ti and N sources. ► A low temperature formation of anatase–rutile heterojunctions has been achieved. ► The nanocatalyst shows an enhanced spectral absorption in visible light region. ► The catalyst owns a high ability for the visible light induced degradation of dye.

Solvothermal syntheses, crystal structures, and properties of new mercury(II)–thioantimonates(III) and a mixed-valent thioantimonate(III,V)

Original Research Article
Pages 287-294
Weiwei Tang, Chunying Tang, Fang Wang, Ruihong Chen, Yong Zhang, Dingxian Jia

Highlights

► Mercury(II)–thioantimonates(III) $[Co(dien)_2]HgSb_2S_5$, $[Ni(dien)_2]HgSb_2S_5$ and $[H_2dien]HgSb_8S_{14}$ and a a mixed-valent thioantimonate(III,V) $[Co(dien)_2]_2Sb_4S_9$ were solvothermally prepared. ► A new μ_3-1κ^2S^1,S^5:2κS^2:3κS^4 bridging coordination mode of the Sb_2S_5 subunit is obtained. ► The mercury(II)–thioantimonates(III) are semiconducting materials with band gaps in 2.04–2.25 eV.

Particle size effects on the magnetic and phonon properties of multiferroic $CoCr_2O_4$

Original Research Article
Pages 295-304
Maciej Ptak, Mirosław Mączka, Krzysztof Hermanowicz, Adam Pikul, Jerzy Hanuza

Graphical abstract

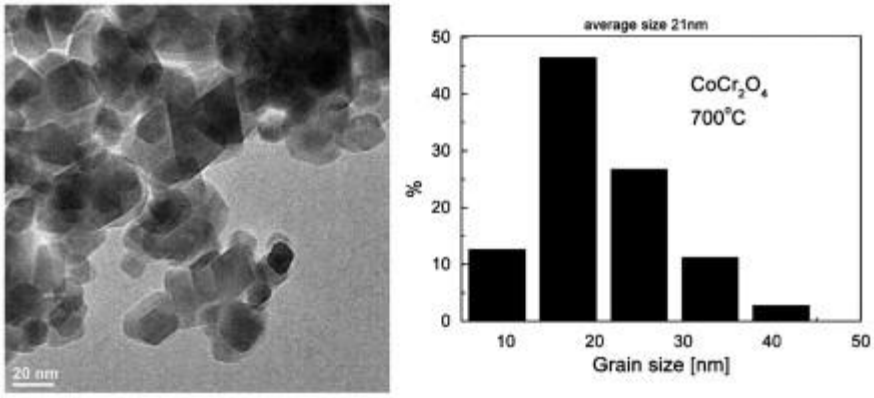

Highlights

► Low-temperature magnetization and IR spectra were measured for two selected samples. ► Magnetization of 4.5 nm particles is significantly different from that of bulk. ► IR spectra revealed pronounced low temperature phonon anomalies. ► We discuss origin of this behavior.

Versatile frameworks constructed from divalent metals with 4,4′-methylenedibenzoic acid and imidazole derivative ligands: Syntheses, crystal structures and physical properties

Original Research Article
Pages 305-316
Guang-Xiang Liu, Xiao-Feng Wang, Hong Zhou

Graphical abstract

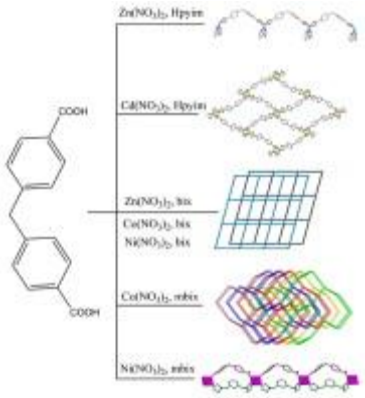

Highlights

► Seven complexes based on 4,4′-methylenedibenzoic acid were obtained. ► The complexes were structurally characterized by single-crystal X-ray diffraction. ► The systematic investigation of the effects of anion and auxiliary N-donor ligands on the ultimate frameworks. ► Complex **1** has modest powder SHG activity and ferroelectric properties.

Preparation of nanoporous titania spherical nanoparticles

Original Research Article
Pages 317-325
Kota Shiba, Soh Sato, Takayuki Matsushita, Makoto Ogawa

Highlights

► Nanoporous titania with variable pore size were obtained by calcination at various temperatures. ► Pore size is determined based on particle shrinkage and growth of crystalline titania domain. ► Nanoporous titania with the same crystallite size and different particle size were obtained.

Structural investigation of α-$LaZr_2F_{11}$ by coupling X-ray powder diffraction, ^{19}F solid state NMR and DFT calculations

Original Research Article
Pages 326-333
Charlotte Martineau, Christophe Legein, Monique Body, Olivier Péron, Brigitte Boulard, Franck Fayon

Graphical abstract

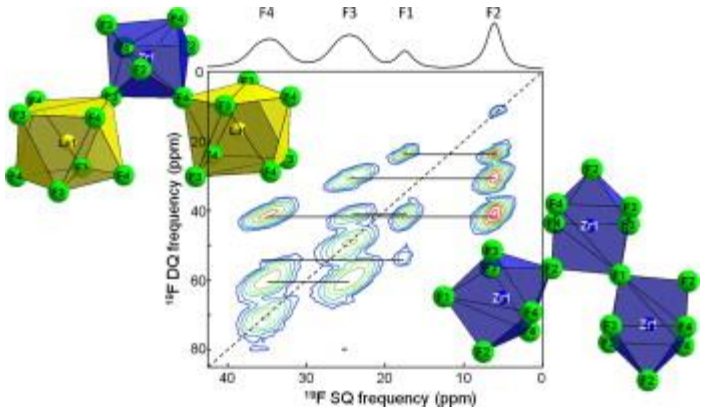

Highlights

► The crystal structure of α-$LaZr_2F_{11}$ has been refined from XRPD data. ► ^{19}F resonances have been assigned using a through-space DQ MAS NMR spectrum. ► ^{19}F chemical shielding tensors have been calculated using the GIPAW method. ► Calculated ^{19}F δ_{iso} and δ_{csa} values are in agreement with experimental values.

Thermal recovery and lattice expansion of self-irradiated $U_{0.80}Am_{0.20}O_{2-x}$, an in situ high temperature x-ray diffraction study

Original Research Article
Pages 334-337
D. Prieur, G. Pagliosa, J. Spino, R. Caciuffo, J. Somers, R. Eloirdi

Graphical abstract

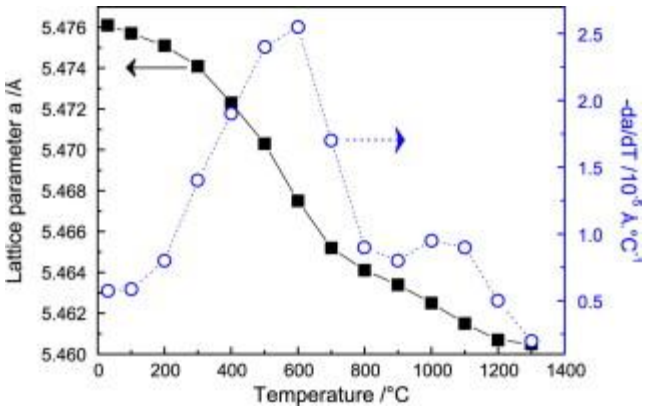

Highlights

► A sample of $U_{0.80}Am_{0.20}O_{2-x}$ has been prepared by sol-gel method and stored for 2 years. ► The recovery of the lattice parameter was studied through an in situ HT-XRD. ► The thermal recovery of the damaged sample (2.2 dpa) showed two maxima at 600 °C and 1000 °C.

Fabrication of superhydrophobic surfaces *via* $CaCO_3$ mineralization mediated by poly(glutamic acid)

Original Research Article
Pages 338-343
Heng Cao, Jinrong Yao, Zhengzhong Shao

Highlights

► Superhydrophobic surfaces were fabricated by a one-step mineralization method. ► $PGlu_{11}$ acted as additive and pre-treatment of substrate was essential for mineralization. ► The surfaces morphology of $CaCO_3$ was controllable. ► The superhydrophobic state was affected by the topology of mineralized surface.